Spin dynamics of the quasi-one-dimensional ferromagnet $CoCl_2 \cdot 2D_2O$

W. Montfrooij, G. E. Granroth, D. G. Mandrus, and S. E. Nagler
Solid State Division, Oak Ridge National Laboratory, Oak Ridge, Tennessee 37831-6393
(Received 4 January 2001; revised manuscript received 18 May 2001; published 13 September 2001)

We present inelastic neutron scattering experiments of the magnetic excitation spectra of $CoCl_2 \cdot 2D_2O$. We find that the excitation energies are well described by the predictions of linear spin-wave theory for a system of weakly coupled ferromagnetic Ising chains. We use the calculated spin-wave intensities to test the (predicted) existence of magnetic Bloch oscillations in this system. We show that these magnetic Bloch oscillations cannot be observed in $CoCl_2 \cdot 2D_2O$.

DOI: 10.1103/PhysRevB.64.134426 PACS number(s): 75.25.+z, 75.50.Dd, 75.60.Ch

I. INTRODUCTION

Recently, Kyriakidis and Loss[1] have predicted that localized magnetic domain walls in anisotropic spin-$\frac{1}{2}$ chains should undergo periodic oscillations. A candidate for the realization of such a system is the magnetic salt $CoCl_2 \cdot 2D_2O$. In this system, the Co atoms form ferromagnetically coupled chains along the *c* axis, with the spins pointing in the *b* direction. Below the Néel temperature ($T_N \sim 17.2$ K), the chains order antiferromagnetically with respect to nearest neighbors, while maintaining ferromagnetic order within the chains. In zero magnetic field, the (solitonlike) domain walls are stable, but delocalized excitations of the ferromagnetic chain. In the presence of a magnetic field along the easy axis, the domain walls are predicted[1] to become localized and to start oscillating along the chain with a finite frequency and amplitude. This form of oscillation is referred to as a magnetic Bloch oscillation, somewhat analogous to the Bloch motion[2] of a band electron in an external field. For a magnetic system, the amplitude of the oscillation is proportional to the bandwidth, which is the degree of exchange anisotropy Δ perpendicular to the direction of magnetization, *z* ($\Delta = J^x - J^y$). Also, the frequency of the oscillation is proportional to the applied magnetic field, whereas the amplitude is inversely proportional to the applied field. This can be seen as a common quantum mechanical phenomenon, in which an oscillation frequency increases with increasing confinement (the latter brought on by the applied field).

The magnetic excitation spectra of $CoCl_2 \cdot 2D_2O$ have been measured by means of far-infrared transmission experiments.[3] This study showed that the system is well described by an effective spin-$\frac{1}{2}$ Hamiltonian, and the anisotropy Δ in the intrachain exchange was found to be 0.16 meV. Subsequent inelastic neutron scattering experiments[4] revealed that some of the exchange parameters extracted from the Raman measurements differed significantly from the inelastic neutron scattering results. In particular, the neutron scattering results showed that the exchange interaction was more Heisenberg like than previously[3] published. However, the model used to analyze the neutron scattering data was only approximate, as it did not take all interactions into account (such as Δ). As a result, there were significant discrepancies between model and experiment.[4]

In this paper, we present neutron scattering experiments on the spin-wave excitations in $CoCl_2 \cdot 2D_2O$ and on the critical scattering near the phase boundaries. We combine these results with published neutron scattering results,[4,5] and analyze the excitations using a more complete interaction model, including the exchange anisotropy Δ which determines the amplitude of the predicted Bloch oscillations in this material. We use the observed spin-wave amplitudes and critical scattering intensities to calculate an upper bound on the existence of Bloch oscillations and discuss the possibility of observing Bloch oscillations in $CoCl_2 \cdot 2D_2O$.

II. EXPERIMENTS AND RESULTS: SPIN WAVES

The neutron scattering experiments were carried out on the triple-axis spectrometers HB1A and HB1, located at the HFIR Reactor of the Oak Ridge National Laboratory. The HB1A spectrometer was operated using a fixed initial energy of 14.7 meV, while the HB1 spectrometer was operated using a fixed final energy of 13.5 meV. For both spectrometers, pyrolytic graphite crystals were used for monochromator and analyzer crystals, while pyrolytic graphite filters (2.5″) were in place to reduce higher-order contamination. An oblong single crystal of approximately 2 g was mounted inside a helium-exchange cryomagnet with the easy axis (*b*) perpendicular to the scattering plane. At $T = 10$ K, we find for the crystallographic parameters $a = 7.1849$ Å, $c = 3.5539$ Å, and $\beta = 97.645°$ (angle between *a* and *c*).

We determined the *H*-*T* phase diagram by following the intensities of ferromagnetic (Fe) $(2n,0,m)$, antiferromagnetic (AF) $(2n+1,0,m)$, and ferrimagnetic (Fi) $(2n/3,0,m)$ Bragg peaks as a function of temperature *T* and magnetic field *H* (see Fig. 1). The intensities of the AF and Fi Bragg peaks are comparable to the nuclear Bragg peak intensities. However, we were unable to identify any magnetic scattering on top of the nuclear Bragg peaks corresponding to a Fe phase at 4.2 K for magnetic fields up to 5.5 T. This is an unexpected result since at low temperatures ($T < 1.6$ K) the phase transition[3] is at $H = 4.49$ T, while the infrared absorption frequencies do not exhibit any marked changes[3] over the entire range $0 < H < 6$ T on raising the temperature to 6 K.

The zero-field Néel temperature of the sample was found to be 17.3 K on a temperature sensor mounted close to the sample (see top panel of Fig. 2). This value is in agreement with the transition temperature of 17.2 K published in the literature,[6] confirming the purity of our sample. For a discussion concerning the critical exponents associated with this

 ©2001 The American Physical Society

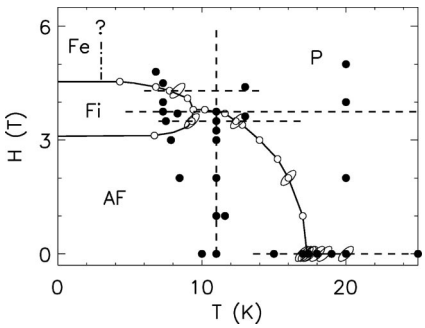

FIG. 1. Magnetic field H vs temperature T phase diagram for $CoCl_2 \cdot 2D_2O$. The solid lines depict the phase boundaries between the paramagnetic (P), antiferromagnetic (AF), ferromagnetic (Fe), and ferrimagnetic (Fi) phases. The open circles are points where we measured these phase boundaries by neutron scattering. The dotted curves at constant T and constant H depict trajectories where we looked (for fixed $\vec{q}$) for scattering associated with the $n=0$ Bloch mode. The solid circles represent points where we carried out measurements as a function of momentum transfer along a^* and/or c^*. The open ellipses are the points where we measured the full scattering function, such as the ones plotted in Fig. 7. The question mark near the Fe phase boundary signifies that we were unable to verify the existence (Ref. 3) of the ferromagnetic phase using neutron scattering.

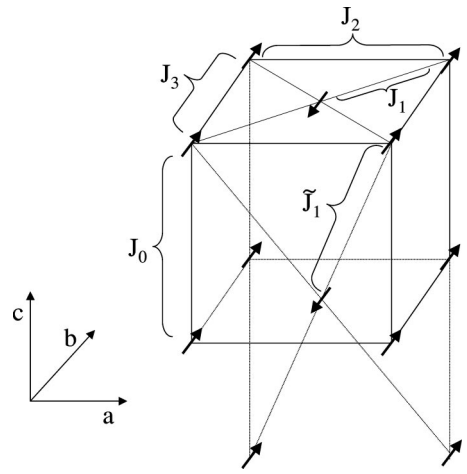

FIG. 3. Antiferromagnetic order in $CoCl_2 \cdot 2D_2O$ and exchange parameters present in the nearest-neighbor Hamiltonian of Eq. (1). The magnetic moments always point along the b direction, and ferromagnetic order within the chains is maintained in all crystal phases (above T_N, only long-range correlations along the chains persist). Note that for every site there are four nearest neighbors interacting through J_1 and $\tilde{J}_1$. We assume the strengths of J_1 and $\tilde{J}_1$ to be equal, since both interactions follow closely related exchange paths.

phase transition, we refer the reader to Ref. 7.

We show some examples of the zero-field spin-wave excitations in the bottom panels of Fig. 2. Well below T_N, the excitations are sharp, while the excitations rapidly broaden upon approaching T_N from below. However, the excitations persist above T_N. This reflects the fact that ferromagnetic order is maintained within the chains on a local scale (about 6 unit cells along c at $T=22$ K). This behavior has been observed before in Ref. 4, where spin-wave excitations were observed up to 130 K. We confirmed that these excitations were magnetic in origin by measuring spectra at much higher momentum transfers, where the magnetic form factor reduces the spin-wave intensity, while the nuclear scattering (if any) is expected to increase in intensity.

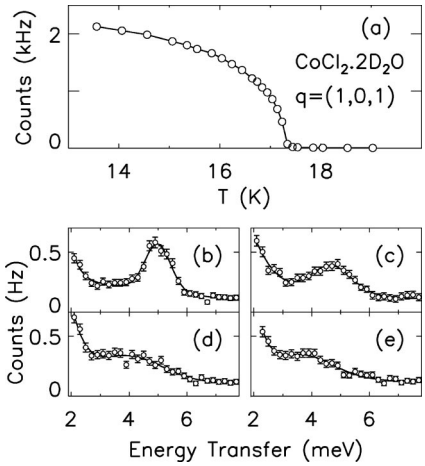

FIG. 2. (a) The temperature dependence of the intensity of the antiferromagnetic Bragg peak $\vec{q}=(1,0,1)$, yielding the Néel temperature T_N of 17.3 K. The four bottom panels depict the variation with temperature of the spin-wave excitation at $\vec{q}=(1,0,0.75)$, uncorrected for any instrumental effects [(b) 10 K, (c) 16 K, (d) 17.4 K, (e) 22 K]. Note the rapid broadening of the excitation as T_N is approached from below and its perseverance above T_N. The solid lines serve as guides to the eye.

We first discuss the results for the spin-wave dispersion in zero field. We use these results to determine the exchange parameters, with the aim of obtaining a reliable measure for the intrachain exchange anisotropy. We analyze our results using an effective spin-$\frac{1}{2}$ Hamiltonian H with nearest-neighbor exchange interactions $J_0, J_1, \tilde{J}_1, J_2$, and J_3 (see Fig. 3). Here we have opted for the same notation as the one used in Ref. 4. Thus we use the following Hamiltonian:

$$H=-\sum_{i,\delta}\left[J^z_\delta S^z_i S^z_{i+\delta}+\frac{1}{2}J^\perp_\delta(S^+_i S^-_{i+\delta}+S^-_i S^+_{i+\delta})+\frac{1}{2}J^a_\delta(S^+_i S^+_{i+\delta}+S^-_i S^-_{i+\delta})\right], \quad (1)$$

where $S^\pm=S^x\pm S^y$ and i runs over the magnetic Co ions. We have chosen the z direction to coincide with the easy axis (b direction). The perpendicular and anisotropic exchange interactions are defined, respectively, as $J^\perp_\delta=(J^x+J^y)/2$ and $J^a_\delta=(J^x-J^y)/2$ with $\delta=0,1,\tilde{1},2,3$.

The Hamiltonian can be diagonalized in the standard manner[8] using linear spin-wave theory, yielding two spin modes (labeled α and β) with excitation energies

$$\omega_{\alpha,\beta}=\sqrt{[Z_1(q)\pm Z_4(q)]^2-[Z_2(q)\pm Z_3(q)]^2}, \quad (2)$$

with

$$Z_1(q)=2J_0^z+2J_2^z+2J_3^z-4J_1^z-4\tilde{J}_1^z-2J_0^{\perp}\cos(\vec{q}\cdot\vec{c})$$
$$-2J_2^{\perp}\cos(\vec{q}\cdot\vec{a})-2J_3^{\perp}\cos(\vec{q}\cdot\vec{b}),$$

$$Z_2(q)=-4J_1^{\perp}\cos(\tfrac{1}{2}\vec{q}\cdot\vec{a})\cos(\tfrac{1}{2}\vec{q}\cdot\vec{b})$$
$$-4\tilde{J}_1^{\perp}[\cos(\tfrac{1}{2}\vec{q}\cdot\vec{a})\cos(\tfrac{1}{2}\vec{q}\cdot\vec{b})\cos(\vec{q}\cdot\vec{c})$$
$$-\sin(\tfrac{1}{2}\vec{q}\cdot\vec{a})\cos(\tfrac{1}{2}\vec{q}\cdot\vec{b})\sin(\vec{q}\cdot\vec{c})],$$

$$Z_3(q)=-J_0^q\cos(\vec{q}\cdot\vec{c})-J_2^q\cos(\vec{q}\cdot\vec{a})-J_3^q\cos(\vec{q}\cdot\vec{b}),$$

$$Z_4(q)=-4J_1^q\cos(\tfrac{1}{2}\vec{q}\cdot\vec{a})\cos(\tfrac{1}{2}\vec{q}\cdot\vec{b})$$
$$-4\tilde{J}_1^q[\cos(\tfrac{1}{2}\vec{q}\cdot\vec{a})\cos(\tfrac{1}{2}\vec{q}\cdot\vec{b})\cos(\vec{q}\cdot\vec{c})$$
$$-\sin(\tfrac{1}{2}\vec{q}\cdot\vec{a})\cos(\tfrac{1}{2}\vec{q}\cdot\vec{b})\sin(\vec{q}\cdot\vec{c})]. \quad (3)$$

The + signs in Eq. (2) refer to the α mode, and the − signs to the mode labeled β. The above equations show that the degeneracy of the spin modes is lifted by the transverse anisotropy of the interaction. Therefore, inelastic neutron scattering experiments can be used to measure the exchange anisotropies. Note that the eigenvalues in Eq. (2) differ from the ones presented in Ref. 4, where the spin-wave energies were calculated using an approximate Green's function formalism and were given by

$$\omega_{\alpha,\beta}=2J_0^z-4J_1^z-4\tilde{J}_1^z-2J_0^{\perp}\cos(\vec{q}\cdot\vec{c})$$
$$\mp 4\cos(\tfrac{1}{2}\vec{q}\cdot\vec{a})\cos(\tfrac{1}{2}\vec{q}\cdot\vec{b})[J_1^q+\tilde{J}_1^q\cos(\vec{q}\cdot\vec{c})]. \quad (4)$$

The − signs in Eq. (4) refer to the α mode, and the + signs to the β mode. Comparing the above expression with Eq. (2), one can see that $Z_2(q)$ and $Z_3(q)$ are not included in Eq. (4).

The intensities of these spin waves in neutron scattering experiments can easily be determined, yielding the familiar result[4] that the weight of the branches in the dynamic structure factor is distributed according to the g tensor, namely,[9]

$$S(\vec{q},\omega)=\frac{1}{2}(1-Q_x^2/Q^2)g_x^2\delta(\omega-\omega_{\alpha})+\frac{1}{2}(1-Q_y^2/Q^2)$$
$$\times g_y^2\delta(\omega-\omega_{\beta})+(1-Q_z^2/Q^2)g_z^2S^z(\vec{q},\omega). \quad (5)$$

Here, $S^z(\vec{q},\omega)$ is the part of the scattering given by the Bloch oscillations, to be discussed in the following section. Using the orientation of the g tensor with respect to the crystalographic axes as determined by Narath[10] [the angle between g_y and c^* is 55° and g_z is parallel to b^*], we find for Q_x and Q_y, respectively,

$$Q_x=h|a^*|\cos(35°-\beta^*)+l|c^*|\cos(35°),$$
$$Q_y=h|a^*|\sin(35°-\beta^*)+l|c^*|\sin(35°). \quad (6)$$

The major axes of the g tensor are[10] $g_x=1.87$, $g_y=3.32$, and $g_z=6.77$. Thus, in general, the observed peak in the neutron scattering measurements is a weighted combination of the position of both branches. We have fitted our neutron scattering results using Eqs. (5) and (6), where we have assumed the exchange interactions J_1 and $\tilde{J}_1$ to be of equal strength since they share identical exchange paths.[4] We plot the results for the magnon frequencies in Fig. 4. We have also included the reported excitation energies from Refs. 4 and 5 in this figure. These latter results equate the peak position with the dominant β mode and might therefore exhibit a (small) systematic error in the region where the two branches differ significantly. As can be seen in Fig. 4, the agreement between experiment and model is good, albeit not perfect ($\chi^2=2$, normalized by degrees of freedom). It is possible that agreement can be improved by including magnetic dipole-dipole interactions,[11] but we have not attempted this here since the obtained agreement is adequate for our present purpose.

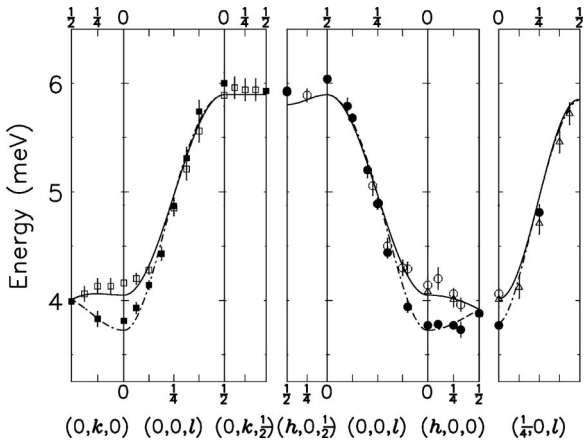

FIG. 4. One-magnon excitation energies in $CoCl_2\cdot 2D_2O$ for $T<7$ K along various directions in reciprocal space. The measurements reported in this paper are denoted by the circles. The results reported in Ref. 4 are given by the squares, and the results of Ref. 5 are given by triangles. For the sake of clarity, measurements at equivalent lattice points have been averaged in the plot. Solid symbols refer to the α mode, open symbols to the β mode (see text). The results of the fitting procedure to the excitation energies for the α and β modes [using Eq. (2)] are given by the solid lines and dashed lines, respectively.

Note that while the two branches cannot be resolved separately (with our energy resolution) at individual q values, the full dispersion curves can nonetheless be determined accurately by measuring in more than one Brillouin zone. On inspecting Eqs. (3), one observes that both $Z_2(q)$ and $Z_4(q)$ change sign upon changing $\vec{q}$ from $(h,0,l)$ to $(1+h,0,l)$, while $Z_1(q)$ and $Z_3(q)$ remain unchanged. This change is equivalent to changing the $\pm$ signs in Eq. (2) into $\mp$ signs. Thus, the observation of the (dominant) β mode at $(1+h,0,l)$ is equivalent to observing the α mode at $(h,0,l)$. Examples of the efficacy of this procedure are given in Ref. 4. In addition, we verified the existence of both branches separately, by choosing such combinations of h and l [see Eq. (6)] that either Q_x/Q or Q_y/Q [see Eq. (5)] were identical to 1, allowing for the observation of a pure β mode or of a pure α mode, respectively.

We compare the present set of exchange parameters as extracted from our model fit to the values published in the

TABLE I. Values for exchange parameters as determined from model fits to the dispersion, compared to the values given in the literature. All values are given in meV. The values for J_1 reported in Ref. 3 have been halved in order to allow for a direct comparison with the present values.

Parameter	Ref. 3	Ref. 4	Current results
$J_0^z-2J_1^z-2\tilde{J}_1^z+J_2^z+J_3^z$	2.30 ± 0.02	2.53 ± 0.03	2.475 ± 0.005
$J_0^\perp$	0.24 ± 0.02	0.48 ± 0.03	0.468 ± 0.006
J_0^a	0.16 ± 0.02	0	0.33 ± 0.06
$J_1^\perp$	-0.0564 ± 0.002	0	-0.12 ± 0.02
J_1^a	-0.032 ± 0.004	-0.02 ± 0.01	0.00 ± 0.005
$J_2^\perp$	-0.024 ± 0.001	0	-0.022 ± 0.007

literature in Table I. The parameters J_2^a, J_3^a, and $J_3^\perp$ were found to be zero within the accuracy of our experiments and have therefore not been included in this table. We find that both $J_0^\perp$ and J_0^a are twice as large as the values reported in Ref. 3, resulting in a doubled estimate[1] for the exchange anisotropy Δ.

Our results are in disagreement with the published values[3,4] for the interchain anisotropy J_1^a (and $\tilde{J}_1^a$). In order to settle this disagreement, we have measured the spin-wave dispersion along $\vec{q}=(h,0,0.25)$. It follows from Eqs. (2) and (3) that the separation between the α and β modes at $l=0.25$ is determined entirely by J_1^a and $\tilde{J}_1^a$ [$Z_3(q)$ is negligible at these wave vectors for all h]. We have followed both α and β modes along $(h,0,0.25)$ and did not observe any separation between the two along this direction within the error bars. Thus, J_1^a and $\tilde{J}_1^a$ are zero to a good approximation. We plot the separation between the two spin-wave modes, as calculated from Eq. (2) (solid line) and Eq. (4) (dashed line), in Fig. 5 for three directions in reciprocal space. Clearly, the present model yields better agreement with the data than the model used in Ref. 4.

III. MAGNETIC BLOCH OSCILLATIONS AND CRITICAL SCATTERING

In order to discuss the (possible) existence of Bloch oscillations in this system, we use Eq. (5) and the intensity of the spin-wave scattering (see Fig. 2) to calculate the expected number of counts for the Bloch oscillations. Kyriakidis and Loss[1] give the following expression for $S^z(\vec{q},\omega)[\vec{q}=(0,0,q)]$ in the presence of a magnetic field b along the easy axis:

$$S^z(q,\omega)=\frac{1}{2}\sum_{n=-N}^{n=N} G_n(q)\,\delta(\omega-n\omega_B), \tag{7}$$

$$G_0(q)=\frac{J_0^2(\zeta)}{\cosh(\beta\omega_B/2)-\cos(q)}, \tag{8}$$

$$G_n(q)=\frac{J_n^2(\zeta)}{2\sin^2(q/2)} \quad (n>0), \tag{9}$$

with $2N+1$ the number of atoms in the chain, $\omega_B=2b$ the Bloch frequency,[1,13] J_n the nth-order Bessel function, $\zeta=(2\Delta/b)|\sin(q)|$, and β is $1/k_BT$. The numerator of Eq. (9) acquires an additional factor $e^{n\beta\omega_B}$ for negative n. Thus, the intensity of the Bloch oscillations depends upon the strength of the magnetic field, upon the temperature, and upon q. Since the full width of the resolution function in energy is roughly 1 meV over the entire energy transfer range of interest ($-2<\omega<6$ meV) for a fixed neutron energy of 14 meV, we can directly compare the spin-wave peak intensity to expected peak intensities for the $n=0$ and $n=1$ Bloch oscillations without the need to resort to elaborate resolution function calculations. A further advantage of the above pro-

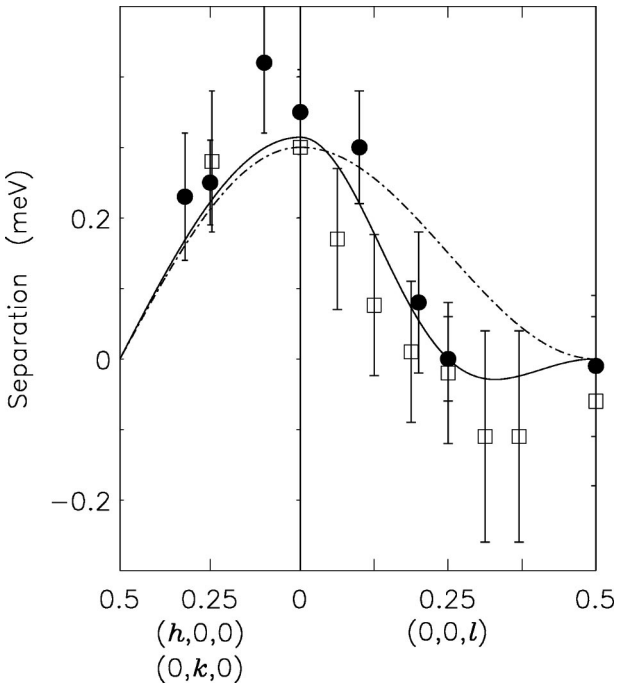

FIG. 5. Separation of the α and β magnon modes in $CoCl_2\cdot 2D_2O$ for $T<7$ K along three directions in reciprocal space. The results for the measurements reported in this paper are denoted by the solid circles, and the results reported in Ref. 4 are given by the open squares. Measurements at equivalent lattice points have been averaged in the plot. The solid line is the calculated separation between the two modes using Eq. (2), while the dashed curve is the calculated separation using the results and spin-wave dispersion [see Eq. (4)] reported in Ref. 4.

cedure is that one effectively corrects for the absorption of neutrons by the sample. Both Co and Cl have a significant absorption cross section for thermal neutrons, resulting in an inverse absorption length of 1.26 cm^{-1} for 14 meV neutrons (that is, about 50% of the neutrons are absorbed traveling through 0.5 cm of the sample, which is a typical length for our scattering geometry). Thus, by comparing the spin-wave intensity for a sample orientation comparable to the orientation in which the presence of Bloch oscillations are being investigated, one can produce a reliable estimate for the expected count rate of the Bloch oscillations.

On the one hand, it turns out that a thermal reactor source is not well suited for identifying any scattering associated with the $n=1$ Bloch oscillation in $CoCl_2 \cdot 2D_2O$, and we were unable to identify this mode. The large amount of incoherent scattering by the sample effectively renders the energy transfer region $\omega < 1$ meV inaccessible to experiment (for fixed initial neutron energy of 14.7 meV), while, for larger energy transfers, the predicted intensity for the Bloch oscillation renders a poor signal to (time independent) background ratio (~ 0.2). We have repeated the experiments using improved resolution with fixed final neutron energies of 10 meV and 6.5 meV. Using the strength of the incoherent peak at zero-energy transfer as a means of normalization between the experiments, we found no signature of a Bloch oscillation for field strengths of $H=1$ T [$\omega_B=2$ meV (Refs. 1 and 13)] and $H=1.8$ T [$\omega_B=1.4$ meV (Refs. 1 and 13)]. For example, at $H=1.8$ T and $\vec{q}=(-1,0,0.25)$ at 13 K, the expected strength is 12 counts per 40 min (our measuring time per point) using the exchange parameters published previously[3] and 60 counts per 40 min using the present exchange parameters. We measure 0 ± 40 counts per 40 min in the signal minus background for all ω within $1 < \omega < 3$ meV. Similar measurements at $T=10$ and 17 K for a variety of magnetic fields strengths were equally inconclusive. Therefore, we conclude that the existence of the $n=1$ Bloch oscillation can neither be confirmed nor ruled out on the basis of our experiments. However, neutron scattering experiments utilizing a cold neutron source (with better energy resolution than can be achieved at a thermal source, allowing for the study of the more intense, lower-frequency Bloch oscillations) should be able to determine the (non)existence of the $n=1$ mode in $CoCl_2 \cdot 2D_2O$.

On the other hand, the (non)existence of the $n=0$ Bloch oscillation can indeed be studied using the present experimental setup. The $n=0$ mode can be observed as the elastic scattering associated with a neutron changing the state of the system $|k\rangle$ (containing a Bloch oscillation of frequency ω_B) into the state $|k+q\rangle$ (still containing a Bloch oscillation of frequency ω_B). This in contrast to the scattering by the $n=1$ mode where the neutron changes the state of the system by either adding a Bloch oscillation of frequency ω_B or by changing the frequency of an existing Bloch oscillation from $n\omega_B$ to $(n+1)\omega_B$. We find that the $n=0$ mode does not exist in $CoCl_2 \cdot 2D_2O$.

The $n=0$ mode is well approximated, for small q, by a Lorentzian line shape, with full width at half maximum (FWHM) Γ along the c axis given by $\Gamma = \beta\omega_B/2\pi$ (in reciprocal lattice units). The amplitude at $q=0$ is 0.11 T^2/ω_B^2 counts per sec (T in kelvin and ω_B in meV), using the same approximation. For example, for $\omega_B=0.5$ meV and $T=17.4$ K, we can expect a count rate of 135 counts per sec, well above the incoherent background of 20 counts per sec (this estimate is not sensitive to the value of Δ). A Bloch oscillation with a frequency of 120 GHz($=0.5$ meV) is predicted[1] to exist in all crystal phases.

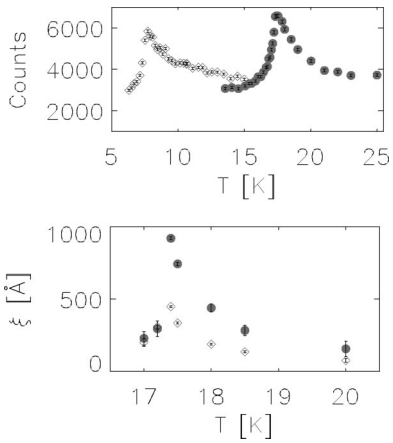

FIG. 6. Critical scattering at 0 T (solid circles) and 4.3 T (diamonds) vs temperature (top panel) for $\vec{q}=(1.17,0,1)$ in counts per 2 min (see trajectories in Fig. 1). This $\vec{q}$ is equidistant between the AF (1,0,1) and Fi ($\frac{4}{3}$,0,1) Bragg peaks so that equivalent amounts of critical scattering are expected to be observed. The incoherent background is roughly 3000 counts per 2 min. The bottom panel depicts the correlation lengths along the a (diamonds) and c directions (solid circles). The correlation length is defined as $\xi = 2\pi/\Gamma$, with Γ the FWHM in reciprocal space.

The maximum of the predicted intensity of the $n=0$ mode coincides with the minimum of the Bloch frequency ω_B. These extremes occur[1] near the phase boundaries shown in Fig. 1. Therefore, in order to be able to ascertain whether the $n=0$ mode exists, we have to identify that part of the scattering which is quasielastic magnetic scattering or critical scattering associated with the onset of three-dimensional order. Fortunately, the critical scattering is easily observable[12] in this sample, with scattering intensities as high as 10 times the incoherent background. We show some of the results in Figs. 6 and 7. We observe the following:

(1) The temperature dependence of the scattering away from the Bragg peak exhibits a cusp behavior, characteristic of critical scattering (see Fig. 6).

(2) The correlation length along the c direction (Fig. 6) remains substantial well above T_N, reflecting that ferrormagnetic order is maintained within the chains. This was also observed in the spin-wave excitations (see Fig. 2). The correlation length along a rapidly decreases above T_N to the order of a couple of unit cells. The correlations along both directions are well described by Lorentzian line shapes.

(3) The orientation of the critical scattering ellipsoid at $H=0$ T in the h-l plane (left panel of Fig. 7) does not coincide with the a direction (the angle between a^* and the axis of the ellipsoid is 15°, while the angle between a and a^* is 7°.6). On increasing the field to 3.5 T (middle panel of

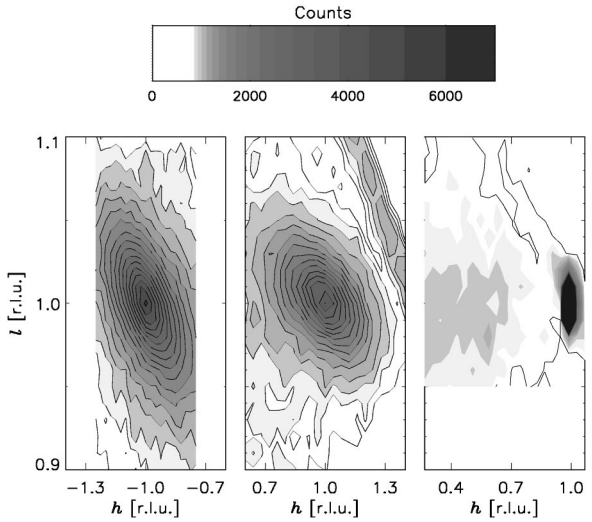

FIG. 7. Critical scattering at $T=17.5$ K, $H=0$ T (left panel), at $T=12.5$ K and $H=3.5$ T (middle), and $T=9.35$ K and $H=3.5$ T (right). All plots share the same grey scale. Note the complete absence of critical scattering or of any scattering associated with the $n=0$ mode near the AF-Fi boundary (right panel). The feature appearing in the top right-hand corner of the middle panel is scattering due to the sample holder.

Fig. 7), a reorientation is observed so that the axis of the ellipsoid is along *a*. However, increasing the field to 4.3 T (not plotted) and measuring the scattering near the ferrimagnetic phase boundary, we find that the axis of the ellipsoid is now oriented along a^*.

(4) The scattering reaches a maximum at the phase boundaries where there is paramagnetic to three-dimensional ordering. No critical scattering was observed at the AF-Fi phase boundary at $H=3.5$ T and $T=9.3$ K (right panel of Fig. 7).

(5) At no point in the Fi phase (see Fig. 1) were we able to distinguish any scattering above the incoherent background.

First, in zero field above T_N the internal field strengths diminish when the order along the *a* and *b* directions is lost. This implies[1,13] that, if anything, ω_B should become smaller with increasing temperature. This would lead to an increase in scattering from the $n=0$ mode with increasing temperature above T_N. The opposite is being observed in Fig. 6. While the scattering as a function of *h* and *l* is well described by a Lorentzian line shape expected for the $n=0$ Bloch mode, the FWHM ($\sim\beta\omega_B$) of the scattering ellipsoid along the *c* direction is expected to narrow with increasing temperature for this $n=0$ mode. Again, we observe the opposite (see Figs. 6 and 7). Therefore, we can safely attribute all of the observed scattering in zero field to critical scattering instead of to the $n=0$ Bloch oscillation, and we can use the shape of the critical scattering to identify similar scattering at other temperatures and magnetic field strengths.

Second, a constant temperature scan ($T=7$ K) with increasing field strength, starting in the AF phase and passing into the Fi phase (see Fig. 1), does not reveal any scattering associated with a $n=0$ Bloch oscillation. We find that the scattering is constant to within 1 count per sec, while at this temperature a count rate of more than 20 counts per sec is expected[1] for the $n=0$ mode near the AF-Fi phase boundary. Thus, the $n=0$ mode does not exist in the AF phase with the predicted intensity. Similarly, we were unable to identify any scattering associated with the $n=0$ mode at any point in the Fi phase in any of our *q* scans (see trajectories in Fig. 1). Invariably, the temperature dependence of the scattering near the paramagnetic to a three-dimensional ordering boundary shows a temperature dependence very similar to the pattern and intensity observed in the scans at zero field (see Fig. 6). Neither a sign of an increased count rate linked to the $n=0$ mode could be observed at expected points (right panel of Fig. 7) nor did the temperature dependence of any of the observed scattering follow the temperature dependence expected for the $n=0$ mode. Therefore, should the $n=0$ Bloch oscillation nonetheless be present, then it must be completely hidden in the incoherent background. However, since the incoherent background is essentially flat upon varying the temperature and magnetic field strength (with the variations less than 5% of the intensity expected for the $n=0$ Bloch oscillation), the $n=0$ Bloch oscillation would then be at least a factor of 20 weaker than predicted.

Finally, scans in the paramagnetic phase for $(-0.2<h<1.2,0,1)$ at $T=20$ K and for field strengths of 0, 2, 4, and 5 T do not show any features identifiable with scattering by the $n=0$ mode. The only feature that can be observed is a weakening of the critical scattering (a small amount is still present at $T=20$ K) with increasing field, reflecting the increased separation from the phase boundary with increasing field (see Fig. 1). However, given that the ferromagnetic order is maintained within the chains (see Figs. 2 and 6), a fairly strong signal could have been expected from the $n=0$ Bloch mode at this temperature. We are thus led to the conclusion that the $n=0$ Bloch oscillations cannot be observed in $CoCl_2\cdot 2D_2O$. By inference, magnetic Bloch oscillations of the form predicted in Ref. 1 do not exist in $CoCl_2\cdot 2D_2O$. Whether the $n=0$ Bloch oscillations may prove to be more different from the $n\neq 0$ Bloch oscillations than predicted (to be verified using a cold neutron source spectrometer) or whether $CoCl_2\cdot 2D_2O$ is simply not a good candidate system for reasons as of yet unknown or even whether magnetic Bloch oscillations do not exist in general remains a topic for future investigation. At present, we do not have an explanation for the (re)orientation of the critical scattering ellipsoid as a function of magnetic field strength.

ACKNOWLEDGMENTS

We thank B. Taylor, S. Moore, C. Redmon, and R. Maples for expert technical assistance during the experiments. Oak Ridge National Laboratory is managed by UT-Battelle, LLC, for the U.S. Department of Energy under Contract No. DE-AC05-00OR22725.

[1] Jordan Kyriakidis and Daniel Loss, Phys. Rev. B **58**, 5568 (1998).
[2] G.H. Wannier, Rev. Mod. Phys. **34**, 645 (1962).
[3] J.B. Torrance, Jr. and M. Tinkham, Phys. Rev. **187**, 587 (1969); **187**, 595 (1969).
[4] J.K. Kjems, J. Als-Nielsen, and Hans Fogedby, Phys. Rev. B **12**, 5190 (1975).
[5] N.B. Christensen, K. Lefmann, I. Johannsen, and O. Jørgensen, Physica B **276**, 784 (2000).
[6] T. Shinoda, H. Chihara, and S. Seki, J. Phys. Soc. Jpn. **19**, 1637 (1964).
[7] Niels Bech Christensen, Ph.D. thesis, University of Copenhagen, Denmark, 2000.
[8] F. Holstein and H. Primakoff, Phys. Rev. **58**, 1048 (1940).
[9] Our definition of $S(q,\omega)$ differs by a factor of 2π from the one presented in Ref. 4, but is identical to the one used in Ref. 1.
[10] A. Narath, Phys. Rev. **140**, A552 (1965).
[11] E. Schlömann, Phys. Rev. **21**, 1312 (1961).
[12] Kjems *et al.* (Ref. 4) did not observe any critical scattering for their sample orientated in the *b*-*c* plane.
[13] The field strength that enters the calculations is the sum of the internal and external fields. The consequence is that the Bloch frequency is expected to decrease with increasing external field strength in the AF and Fi phases, and increase with increasing external field strength in the Fe phase (see Ref. 1). Thus, $\omega_B(H=1\ \mathrm{T})=2$ meV, $\omega_B(H=1.8\ \mathrm{T})=1.4$ meV, and $\omega_B(H=3\ \mathrm{T})=0.5$ meV.